Int. J. Electrochem. Sci., 17 **(2022)** Article Number: 221173, doi: 10.20964/2022.11.81

International Journal of
ELECTROCHEMICAL
SCIENCE
www.electrochemsci.org

Synthesis of Fe_2O_3/rGO Based Composites as Anode material for Lithium ion batteries using sewage sludge as source of Iron (III) oxide

Jing Li[1,*], *Li Yan*[2,3]

[1] Department of Chemistry and Environmental Engineering, Hebei Chemical & Pharmaceutical College, ShiJiazhuang 050000,China
[2] School of aeronautics, Chongqing Jiaotong University, Chongqing, 400074, China;
[3] The Green Aerotechnics Research Institute of CQJTU, Chongqing, 401174, China
[*]E-mail: lisalj_2008@126.com, YanLi@cqjtu.edu.cn

Received: 24 August 2022 / *Accepted:* 9 October 2022 / *Published:* 20 October 2022

The current study focused on creating ferric oxide from oily sewage sludge through a hydrothermal reaction and creating a composite of ferric oxide and reduced graphene oxide (Fe_2O_3/rGO) through a hydrothermal reaction in order to study the electrochemical behavior of the composite as an anode aimed at a high-performance Li-ion battery. The successful synthesis of the Fe_2O_3/rGO composite using the hydrothermal process was demonstrated by morphological and structural analyses by SEM and XRD. It was also demonstrated that γ-Fe_2O_3 particles were dispersed on the wrinkled surface of the rGO nanosheets, which can increase the active surface and facilitate electrochemical reactions by providing a path for Li-ions to permeate from the electrolyte to the solid electrode. Study the electrochemical properties of Fe_2O_3/rGO composite as anode in electrochemical cell showed a reversible discharge capacity of 1250 $mAhg^{-1}$ after 100 cycles at a density of 0.1 Ag^{-1} with coulombic efficiency of 96%, which indicted to better or appropriate performance in Fe_2O_3/rGO composite in comparison with the other reported electrode for Li-ion batteries because of synergetic effect of γ-Fe_2O_3 and rGO nanosheets to enhances in the active surface and facilitates the electrochemical reaction between Fe_2O_3 and Li^+ ions. Results of the rate performance of the Fe_2O_3/rGO nanocomposite electrode under various current densities from 0.1 Ag^{-1} to 2 Ag^{-1} at room temperature demonstrated great rate performance and very stable cycling performance.

Keywords: Hydrothermal Synthesis; Ferric Oxide; Reduced Graphene Oxide; Composite; Li-Ion Battery; Cycling performance

1. INTRODUCTION

The fact that the global Li-ion battery market is seeing a spike shows how vital Li-ion batteries are to the globe as energy storage technologies [1, 2]. These batteries currently rule the portable

electronics and electric car industries as well as the automotive industry [3, 4]. Applications in the military and aerospace are becoming more and more common [5, 6]. These batteries are frequently used for electric tools, medical equipment, homes, building and logistics, emergency preparedness, and other purposes [7, 8]. Additionally, it is utilized in the production of glass and ceramics, as well as the batteries for cell phones and computers. Another significant application that is expected is storage in electrical grids [9, 10].

Li-ion batteries have the best energy density of any battery cell thanks to lithium, an incredibly light metal [11-13]. As a result, they have a higher energy capacity than alkaline batteries or any other single-use battery of a similar size. They may simply pack more power cells than Li-polymer batteries because of their exceptional performance in hot and cold environments [14-16]. This feature is used by smartphone manufacturers to increase power while keeping a sleek design profile. Li-ion batteries are also more stable and can be recharged hundreds of times [17-19]. Compared to other rechargeable batteries, they often have a better energy density, higher voltage capacity, and a lower self-discharge rate [20]. A single cell has a longer charge retention than other battery types, which improves power efficiency [21, 22].

Graphite, the principal substance used for one of the two electrodes known as the anode, is a crucial component of Li-ion batteries. Li-ions go through an electrolyte buffer that separates the cathode and anode of a battery as it charges [23-25]. However, graphene batteries are a new technology that enable higher electrode densities, quicker cycle times, and the capacity to keep the charge for a longer period of time, all of which extend the battery's longevity [26-28]. There are numerous varieties of established graphite batteries [29, 30]. Studies have shown that one of the most successful ways to improve Li-ion batteries is to synthesize hybrid nanomaterials containing carbon nanostructures like graphene and CNTs [31-36]. In order to explore the electrochemical behavior of the composite as an anode aimed at a high-performance Li-ion battery, the current work was carried out to prepare ferric oxide from oily sewage sludge and hydrothermally synthesize Fe_2O_3/rGO. The novelty of this work is the utilization of sewage as the raw material for preparing ferric oxide, which could offer the benefits of reducing the volume of sludge for disposal and management.

2. EXPERIMENT

2.1 Preparation of the ferric oxide from oily sewage sludge

Sludge was supplied by Baosteel Group Corporation in Shanghai Province, China, from oily sewage sludge. The sludge was kept at -10°C to reduce microbial activity, however this could cause the sample to deteriorate for 24 hours. Samples were then dried in the sun for 72 hours. The primary chemical makeup of the sun-dried sample is displayed in Table 1. In a hydrothermal reaction, ferric oxide powder was created [37]. First, 20 g of sun-dried samples were acid leached in 20 ml of a 5 M sulfuric acid (97%, Merckmillipore, Germany) solution at 80 °C for 5 hours under vigorous magnetic stirring. Then, a solvent-oil solution was separated from the sludge by filtration. The sludge was dispersed twice with the acid solvent to extract any remaining oil. After this extra chemical process, the iron phase in the sludge became iron sulfate. The sludge was oxidized by 20 ml of hydrogen peroxide (30 wt.%, Sigma-Aldrich). After then, 5 ml of ammonia (99.98%, Sigma-Aldrich) was added to the hydrogen peroxide solution under vigorous magnetic stirring to get the solution to have a pH of

7. In order to produce ferric hydroxide, the magnetic stirring was continued for 60 minutes. The resulting red-brown precipitates were then filtered, and 10 ml of NaOH solution (97.0%, Sigma-Aldrich) was added. The final step involved moving the finished product into a Teflon-lined hydrothermal reactor for 120 minutes at 70° C. After cooling, the product was combined with deionized water to separate and wash the ferric oxide powder, and the resulting suspension was centrifuged three times. The resulting ferric oxide powders were then dried for eight hours in a vacuum oven at 75 °C.

Table 1. Main chemical composition of sun-dried samples obtained by chemical analysis.

Component	**Content (wt. %)**
Fe	74.92
Mn	0.17
Cr	0.06
Si	0.05
Ni	0.04
V	0.01
Oil	15.40
other	9.35

2.2 Preparation of ferric oxide/reduced graphene oxide based composites

The Fe_2O_3/rGO composite was synthesized through a hydrothermal process [38, 39]. 1 g of the obtained Fe2O3 powders was mixed with 10 ml of GO (98wt%, Xiamen Tob New Energy Technology Co., Ltd., China) solution, 0.5 g of terephthalic (98%, Sigma-Aldrich), 0.6 g polyvinylpyrrolidone (≥99.0%, Sigma-Aldrich) and 65 mL of N,Ndimethylformamide (≥99.0%, Sigma-Aldrich). To get the yellow precipitate, the mixture was agitated for 35 minutes. It was then transported into a hydrothermal reactor with a Teflon lining and heated to 145°C for 10 hours. After cooling, the product was combined with ethanol to separate and wash the precipitate, and the resulting suspension was centrifuged three times. The goods were then dried in a vacuum oven for four hours at 55 °C. To create the Fe_2O_3/rGO composite, the resultant yellow powder was next heated at 350 °C for 120 minutes at a rate of 10 °C/min.

2.2. Characterizations

Morphological and structural analyses of materials were performed by scanning electron microscopy (SEM, FEI Model Quanta 450 FEG, Hillsboro, OR, USA) and X-ray diffraction (XRD; MiniFlex-600, Rigaku Corporation, Tokyo, Japan), respectively. Chemical analysis of the obtained powder of a sun-dried oily sewage sludge sample was performed to examine the ferrous and ferric ion concentrations, according to the GB/T 1863-2008 (China Industrial Standard). All electrochemical

measurements were conducted on 2032-type coin cells as the working electrode which were fabricated from hydrothermal synthesized Fe2O3/rGO composite that the punched into circular discs and assembled in an Ar-filled glove box (MBraun, Unilab, Germany) using the Li-metal disc as the counter electrode and reference electrode. The Celgard@2325 membrane was used as the separator. The electrolyte was prepared from 1 M LiPF6 (≥99.99%, Sigma-Aldrich) mixed with ethylene carbonate (≥99%, Sigma-Aldrich) and diethyl carbonate (99%, Sigma-Aldrich) equal volume ratio. The cyclic voltammetry (CV) measurements were at a scan rate of 0.1 mV/s in the voltage range from 0.0 to 3.0 V (vs Li/Li^+) using an electrochemistry workstation (CS1005, Zhengzhou CY Scientific Instrument Co., Ltd., China) at room temperature. The galvanostatic charge/discharge tests, rate performance and cycling stability were carried out on Neware battery testing system (CT-3008W-S4, China).

3. RESULTS AND DISCUSSION

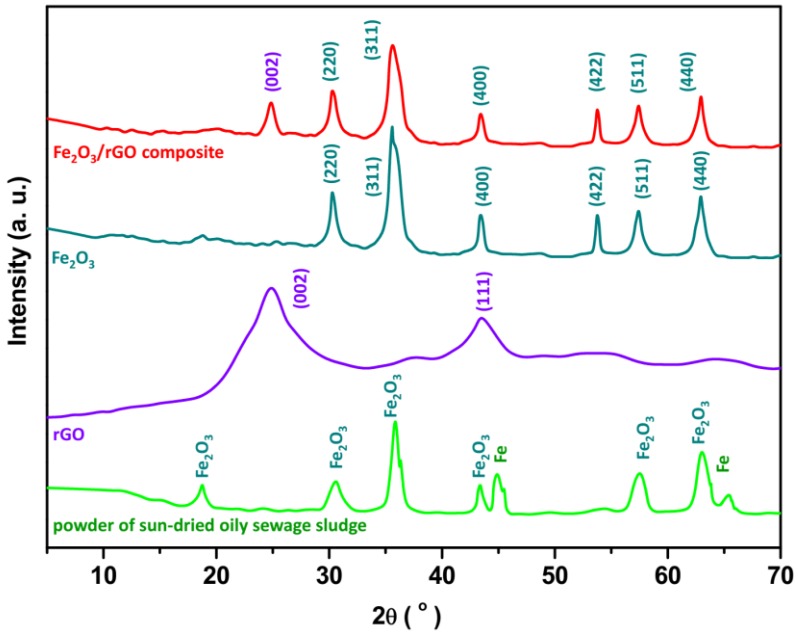

Figure 1. XRD profiles of powders of sun-dried oily sewage sludge sample, rGO, synthesized Fe_2O_3 and Fe2O3/rGO composite.

Figure1 shows the results of determination the phase purity and crystallinity powders of sun-dried oily sewage sludge sample, rGO, synthesized Fe_2O_3 and Fe_2O_3/rGO composite. As seen from Figure 1a, XRD patterns of the sun-dried oily sewage sludge sample indicate the presence of the most abundant iron phases of Fe_2O_3 and pure iron (Fe) according to JCPDS cards No. 25-1402 and 65-4899, respectively. The XRD profile of rGO exhibits characteristic diffraction peaks at 24.92° and 43.59° which are assigned to (002) and (111) planes of the graphitic structure of rGO, respectively [40-42]. The XRD profile of Fe2O3 shows characteristic sharp diffraction peaks at 30.17°, 35.57°, 43.44°, 53.73°, 5730°, and 62.88°, which are assigned to the index diffractions of the tetragonal phase -Fe2O3 (220), (311), (400), (422), (511), and (440) planes (JCPDS card No. 25-1402) [43-45]. XRD profile of Fe2O3/rGO composite depicts the both diffraction peaks of γ-Fe_2O_3 and rGO, indicating that the Fe2O3/rGO composite was successfully synthesized using a hydrothermal process.

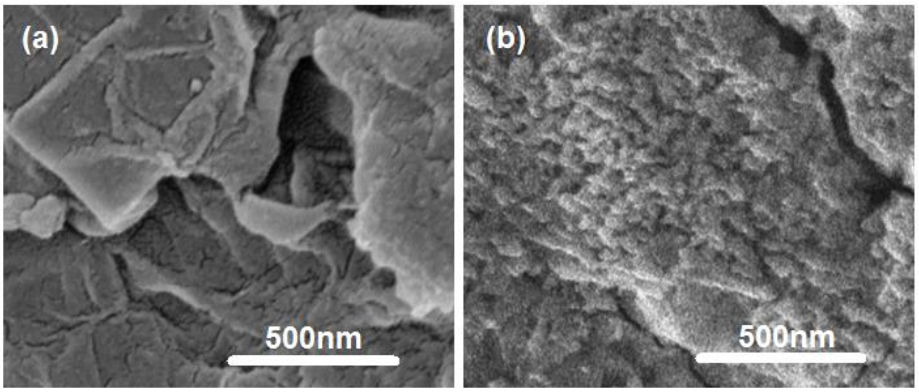

Figure 2. SEM micrographs of (a) rGO, (b) Fe_2O_3/rGO composite.

SEM micrographs in Figure 2 display the morphological structures of rGO and Fe_2O_3/rGO composite, respectively. The SEM micrograph of rGO indicates wrinkled and folded rGO nanosheets with overlapped structures. As seen, rGO exhibits a good lamellar structure separated by free spaces. SEM micrograph of Fe_2O_3/rGO composite demonstrates to γ-Fe_2O_3 particles are dispersed on the wrinkled surface of the rGO nanosheets. It is observed that the rGO nanosheets limit the agglomeration of γ-Fe_2O_3 particles, thereby the average size of γ-Fe_2O_3 particles decorated on rGO nanosheets is 75 nm. It can be seen that the surface of the Fe_2O_3/rGO composite has micro-pores, which increase the active surface and facilitate the electrochemical reaction by providing a path for Li ions to permeate from the electrolyte to the solid electrode and increase the effective liquid-solid interfacial area [46].

Figure 3 depicts the CV curves of Fe_2O_3/rGO composite as anode in electrochemical cell with Li metal as the counter electrode at voltage range of 0.0-3.0V and a 0.1mV/s scan rate which illustrated to typical CV curves of Fe_2O_3 based anode materials in Li-ion batteries [47-49]. In the 1st cycle, a sharp cathodic peak is observed at 0.59 V which attributed to insertion of Li^+ ion in γ-Fe_2O_3 and the electrochemical formation of amorphous Li_2O [50-52]. Moreover, weak plateaus were observed between 1.5 and 1.8 V during 1st anodic scan which related to the oxidation of Fe to Fe^{3+} to reform Fe_2O_3 [50, 53, 54]. As expected, the CV curves exhibit important differences between the first and following cycles. As seen, the strong peak at 0.59 V disappeared after the 1st cycle, implying an irreversible process for formation of the solid-electrolyte-interphase (SEI) layer [55, 56]. During the 2nd and 3rd CV, an extended cathodic peak at 0.84 V is depicted which is attributed to the reversibility and good capacity stability [46, 57]. The broadening of the reduction peak after the first cycle can be associated with the amorphous nature/ crystal structure destruction of the active material of the electrode [58-60].

The different cycles of discharge and charge curves of cell at 0.1Ag^{-1} current density and at room temperature are depicted in Figure 4. The results show the good agreement between the discharge and charge and CV measurements due to the presence of a plateau at 0.76 V in the first discharge curves, corresponding to the peaks in c cycle of CV curves, implying the reduction of Fe ions to form Fe metal (Fe^0) and amorphous Li_2O [61-63]. In the following discharge curves, the plateau shifts to 0.9 V that it can be associated with the change the crystal structure in first lithiation [64, 65]. It is observed that after charge the discharged Fe_2O_3/rGO composite electrode to 3.0 V, there

is a smooth voltage curve until 1.5 V. It is accompanied by a rising slope up to 3.0 V, indicating the regeneration of Fe_2O_3 [50, 53].

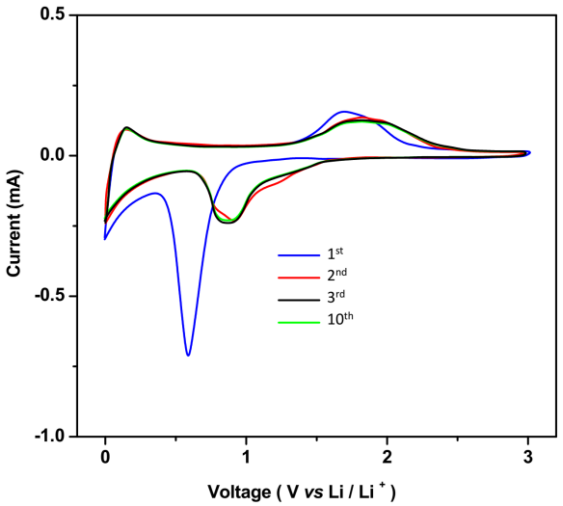

Figure 3. The CV curves of Fe_2O_3/rGO composite as anode in electrochemical cell with Li metal as the counter electrode at voltage range of 0.0-3.0V and a 0.1mV/s scan rate

Results show that during the first cycle, the anode delivers high discharge and charge capacity values of 1750 and 1155 $mAhg^{-1}$, respectively, and the coulombic efficiency reaches 66%. The first cycle's discharge capacity is significantly greater than the second cycle (1214 $mAhg^{-1}$) which indicated to irreversible capacity of 536 $mAhg^{-1}$ due to SEI formation and the charge consumption in irreversible electrochemical reactions between anode material and Li^+ ions [66-68].

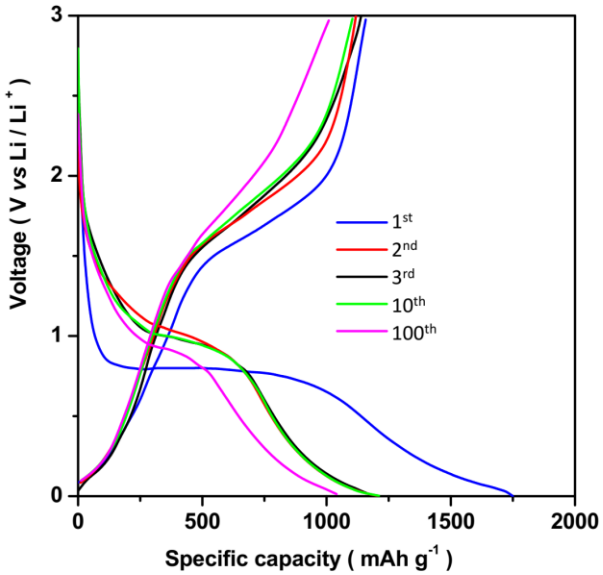

Figure 4. The different cycles of discharge and charge curves of cell at 0.1Ag^{-1} current density and at room temperature

Figure 5 shows the discharge capacity curves of rGO, commercial Fe_2O_3 and Fe_2O_3/rGO composite electrodes versus cycle number at a current density of 0.1 Ag^{-1}. As seen, rGO and

commercial Fe_2O_3 show discharge capacities of 253 $mAgh^{-1}$ and 141 $mAhg^{-1}$ after 100 cycles, respectively. Fe_2O_3/rGO composite shows capacity decay in the 1st cycle, but it displays reasonable Li storage capability and cycle performance during 100 cycles. A high discharge capacity of 1250 $mAhg^{-1}$ is retained during 100 cycles. At the same time, the coulombic efficiency of the 1st cycle (48%) is increased to 97% in the 2nd cycle. The coulombic efficiency of the cell remains at approximately 96% in the following cycles (Figure 6).

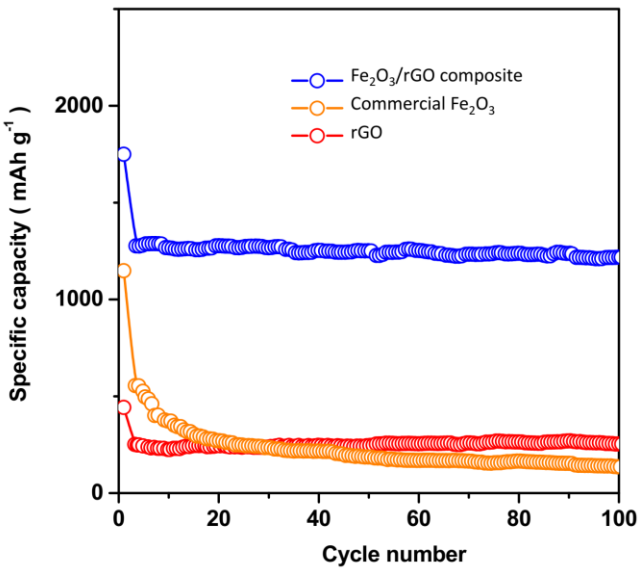

Figure 5. The discharge capacity curves of rGO, commercial Fe_2O_3 and Fe_2O_3/rGO composite electrodes curves versus cycle number at 0.1Ag^{-1} current density.

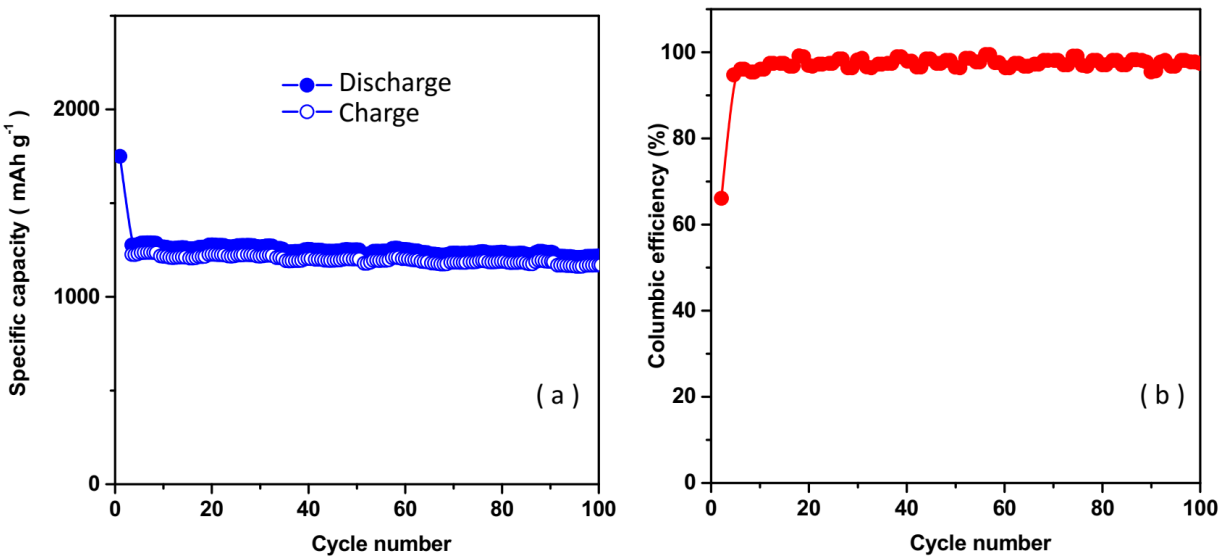

Figure 6. (a) Discharge/charge capacities and (b) coulombic efficiency versus cycle number of Fe_2O_3/rGO composite at the current density of 0.1 Ag^{-1} between 3 and 0 V.

Table 2 compares the electrochemical performance of the Fe2O3/rGO composite electrode to the electrochemical performance of various reported electrodes for Li-ion batteries, indicating that the synergetic effect of γ-Fe_2O_3 and rGO nanosheets provides the better or appropriate performance in Fe_2O_3/rGO composite. The discharge capacity of Fe_2O_3/rGO composite is also greater than the theoretical capacity of Fe_2O_3 (1007 $mAhg^{-1}$), demonstrating that γ-Fe_2O_3 particles decorated on rGO nanosheets can increase the Li storage capability due to enhances in the active surface and facilitates the electrochemical reaction between Fe_2O_3 and Li^+ ions [69]. Additionally, a stable SEI film can be generated on the surface of rGO nanosheets [70].

Table 2. The comparison between the electrochemical performance of Fe_2O_3/rGO composite electrode and various recent reported electrode for Li-ion batteries.

Electrode	**Specific capacity (mAh g^{-1})**	**Cycle**	**Current density (mA g^{-1})**	**Ref.**
Carbon nanotubes grown on graphene paper	290	40	30	[31]
α-Fe_2O_3 nanofibers	1293	40	60	[71]
Fe_2O_3 microboxes	950	30	200	[72]
Graphene nanosheets	834	15	50	[73]
α-Fe_2O_3 hollow spheres	750	100	200	[74]
α-Fe_2O_3 nanocapsules	740	30	0.1 C	[75]
Graphene paper	~200	15	100	[32]
Fe_2O_3@C composites	600	100	200	[76]
Nitrogen-doped graphene anchored on graphite foam	396	300	186	[77]
Fe_2O_3/rGO composite	1250	100	100	Present study

Rate capability has always been an important factor in the design of Li-ion batteries. Figure 7 shows results of rate performance of Fe_2O_3/rGO nanocomposite electrode under various current density from 0.1 Ag^{-1} to 2 Ag^{-1} at room temperature.

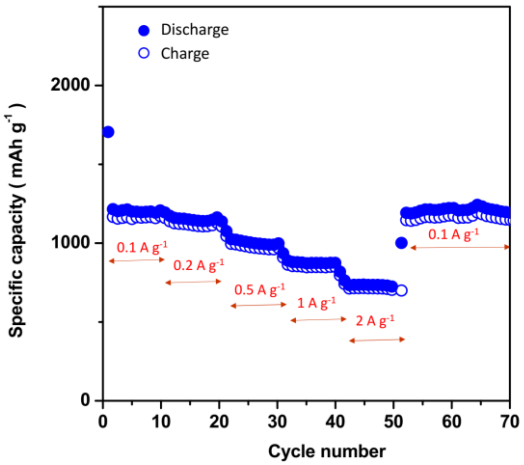

Figure 7. Results of study the rate performance of Fe_2O_3/rGO nanocomposite electrode under various current density from 0.1 Ag^{-1} to 2 Ag^{-1} at room temperature.

It demonstrates a great rate of performance. As observed, the discharge value of 7 $mAhg^{-1}$ is obtained at high rate of 2 Ag^{-1}. When the rate is restored to 0.1 Ag^{-1} after cycling at different rates, the specific capacity of the Fe_2O_3/rGO composite electrode can be recovered 1119 $mAh\ g^{-1}$, which illustrates very stable cycling performance.

4. CONCLUSION

In conclusion, this work demonstrated the hydrothermal synthesis of Fe_2O_3 from oily sewage sludge and the hydrothermal fabrication of Fe_2O_3/rGO composite using the generated Fe_2O_3. The hydrothermal technique used to create the Fe_2O_3/rGO composite was successfully demonstrated by morphological and structural investigations. Study the electrochemical behavior of composite as anode for high-performance Li-ion battery showed a reversible discharge capacity of 1250 $mAhg^{-1}$ after 100 cycles at a density of 0.1 Ag^{-1} with coulombic efficiency of 96%, which indicted to better or appropriate performance in Fe_2O_3/rGO composite in comparison with the other reported electrode for Li-ion batteries because of synergetic effect of γ-Fe_2O_3 and rGO nanosheets. Results of the rate performance of the Fe_2O_3/rGO nanocomposite electrode under various current densities from 0.1 Ag^{-1} to 2 Ag^{-1} at room temperature demonstrated great rate performance and very stable cycling performance.

References

1. V. Etacheri, R. Marom, R. Elazari, G. Salitra and D. Aurbach, *Energy & Environmental Science*, 4 (2011) 3243.
2. X. Zhang, Y. Tang, F. Zhang and C.S. Lee, *Advanced energy materials*, 6 (2016) 1502588.
3. J. Neumann, M. Petranikova, M. Meeus, J.D. Gamarra, R. Younesi, M. Winter and S. Nowak, *Advanced energy materials*, 12 (2022) 2102917.
4. X. Tong, F. Zhang, B. Ji, M. Sheng and Y. Tang, *Advanced Materials*, 28 (2016) 9979.
5. Z. Said, M. Ghodbane, B. Boumeddane, A.K. Tiwari, L.S. Sundar, C. Li, N. Aslfattahi and E. Bellos, *Solar Energy Materials and Solar Cells*, 239 (2022) 111633.
6. H. Karimi-Maleh, H. Beitollahi, P.S. Kumar, S. Tajik, P.M. Jahani, F. Karimi, C. Karaman, Y. Vasseghian, M. Baghayeri and J. Rouhi, *Food and Chemical Toxicology*, (2022) 112961.
7. J. Baars, T. Domenech, R. Bleischwitz, H.E. Melin and O. Heidrich, *Nature Sustainability*, 4 (2021) 71.
8. B. Ji, F. Zhang, X. Song and Y. Tang, *Advanced materials*, 29 (2017) 1700519.
9. D. Choi, N. Shamim, A. Crawford, Q. Huang, C.K. Vartanian, V.V. Viswanathan, M.D. Paiss, M.J.E. Alam, D.M. Reed and V.L. Sprenkle, *Journal of Power Sources*, 511 (2021) 230419.
10. Z. Said, S. Arora, S. Farooq, L.S. Sundar, C. Li and A. Allouhi, *Solar Energy Materials and Solar Cells*, 236 (2022) 111504.
11. J.W. Choi and D. Aurbach, *Nature Reviews Materials*, 1 (2016) 1.
12. M. Wang, C. Jiang, S. Zhang, X. Song, Y. Tang and H.-M. Cheng, *Nature chemistry*, 10 (2018) 667.
13. B. Li, C. Li, Y. Zhang, Y. Wang, D. Jia and M. Yang, *Chinese Journal of Aeronautics*, 29 (2016) 1084.
14. S. Mu, Q. Liu, P. Kidkhunthod, X. Zhou, W. Wang and Y. Tang, *National science review*, 8 (2021) nwaa178.

15. D. Jia, Y. Zhang, C. Li, M. Yang, T. Gao, Z. Said and S. Sharma, *Tribology International*, 169 (2022) 107461.
16. H. Karimi-Maleh, C. Karaman, O. Karaman, F. Karimi, Y. Vasseghian, L. Fu, M. Baghayeri, J. Rouhi, P. Senthil Kumar and P.-L. Show, *Journal of Nanostructure in Chemistry*, (2022) 1.
17. K. Wang, J. Wan, Y. Xiang, J. Zhu, Q. Leng, M. Wang, L. Xu and Y. Yang, *Journal of Power Sources*, 460 (2020) 228062.
18. T. Wei, Z. Wang, M. Zhang, Q. Zhang, J. Lu, Y. Zhou, C. Sun, Z. Yu, Y. Wang and M. Qiao, *Materials Today Communications*, 31 (2022) 103518.
19. T. Gao, C. Li, Y. Wang, X. Liu, Q. An, H.N. Li, Y. Zhang, H. Cao, B. Liu and D. Wang, *Composite Structures*, 286 (2022) 115232.
20. C. Weng, X. Sun, B. Han, X. Ye, Z. Zhong, W. Li, W. Liu, H. Deng and Z. Lin, *Journal of hazardous materials*, 393 (2020) 122296.
21. A. Tomaszewska, Z. Chu, X. Feng, S. O'kane, X. Liu, J. Chen, C. Ji, E. Endler, R. Li and L. Liu, *ETransportation*, 1 (2019) 100011.
22. C. Zhao, M. Xi, J. Huo and C. He, *Physical Chemistry Chemical Physics*, 23 (2021) 23219.
23. J.B. Goodenough and K.-S. Park, *Journal of the American Chemical Society*, 135 (2013) 1167.
24. B. Meng, J. Wang, L. Yang, M. Chen, S. Zhu and F. Wang, *Journal of Materials Science & Technology*, 132 (2023) 69.
25. L. Tang, Y. Zhang, C. Li, Z. Zhou, X. Nie, Y. Chen, H. Cao, B. Liu, N. Zhang and Z. Said, *Chinese Journal of Mechanical Engineering*, 35 (2022) 1.
26. K. Cai, X. Jing, Y. Zhang, L. Li and X. Lang, *International Journal of Energy Research*, 46 (2022) 14570.
27. J. Kang, Y. Xue, J. Yang, Q. Hu, Q. Zhang, L. Gu, A. Selloni, L.-M. Liu and L. Guo, *Journal of the American Chemical Society*, 144 (2022) 8969.
28. P. Shandilya, P. Mandyal, V. Kumar and M. Sillanpää, *Separation and Purification Technology*, 281 (2022) 119825.
29. Y.E. Durmus, H. Zhang, F. Baakes, G. Desmaizieres, H. Hayun, L. Yang, M. Kolek, V. Küpers, J. Janek and D. Mandler, *Advanced energy materials*, 10 (2020) 2000089.
30. J. Zhang, C. Li, Y. Zhang, M. Yang, D. Jia, G. Liu, Y. Hou, R. Li, N. Zhang and Q. Wu, *Journal of Cleaner Production*, 193 (2018) 236.
31. S. Li, Y. Luo, W. Lv, W. Yu, S. Wu, P. Hou, Q. Yang, Q. Meng, C. Liu and H.M. Cheng, *Advanced Energy Materials*, 1 (2011) 486.
32. Y. Hu, X. Li, D. Geng, M. Cai, R. Li and X. Sun, *Electrochimica Acta*, 91 (2013) 227.
33. R. Jiang, X. Luo and X. Wen, *International Journal of Electrochemical Science*, 11 (2016) 9471.
34. C. Fu, G. Zhao, H. Zhang and S. Li, *International Journal of Electrochemical Science*, 8 (2013) 6269.
35. D. Zhang, J. Qiao, X. Dong, B. Xu, R. Li and C. Chang, *International Journal of Electrochemical Science*, 13 (2018) 1744.
36. G. Alam, I. Ihsanullah, M. Naushad and M. Sillanpää, *Chemical Engineering Journal*, 427 (2022) 130011.
37. B. Liu, S.-g. Zhang, D.-a. Pan and C.-c. Chang, *Procedia Environmental Sciences*, 31 (2016) 653.
38. D. Bengono, B. Zhang, Y. Yao, L. Tang, W. Yu, J. Zheng, D. Chu, J. Li and H. Tong, *Ionics*, 26 (2020) 1695.
39. R. Vinayagam, N. Dave, T. Varadavenkatesan, N. Rajamohan, M. Sillanpää, A.K. Nadda, M. Govarthanan and R. Selvaraj, *Chemosphere*, 296 (2022) 133965.
40. S.A. Soomro, I.H. Gul, H. Naseer, S. Marwat and M. Mujahid, *Current Nanoscience*, 15 (2019) 420.
41. L. Yang, Q. Dai, L. Liu, D. Shao, K. Luo, S. Jamil, H. Liu, Z. Luo, B. Chang and X. Wang,

Ceramics International, 46 (2020) 10917.
42. Z. Said, M. Jamei, L.S. Sundar, A. Pandey, A. Allouhi and C. Li, *Journal of Molecular Liquids*, 347 (2022) 117944.
43. J. Yang, H. Zhang, M. Yu, I. Emmanuelawati, J. Zou, Z. Yuan and C. Yu, *Advanced Functional Materials*, 24 (2014) 1354.
44. Y. Wang, C. Li, Y. Zhang, M. Yang, B. Li, L. Dong and J. Wang, *International Journal of Precision Engineering and Manufacturing-Green Technology*, 5 (2018) 327.
45. Y. Zhou, W.-b. Li, V. Kumar, M.C. Necibi, Y.-J. Mu, C.-z. Shi, D. Chaurasia, S. Chauhan, P. Chaturvedi and M. Sillanpää, *Environmental Research*, 211 (2022) 113075.
46. M. Aadil, W. Shaheen, M.F. Warsi, M. Shahid, M.A. Khan, Z. Ali, S. Haider and I. Shakir, *Journal of Alloys and Compounds*, 689 (2016) 648.
47. B.-S. Wu, P. Wang and J. Song, *Journal of Materials Science: Materials in Electronics*, 31 (2020) 6779.
48. Y. Chen, J. Long, B. Xie, Y. Kuang, X. Chen, M. Hou, J. Gao, H. Liu, Y. He and C.-P. Wong, *ACS Applied Materials & Interfaces*, 14 (2022) 4647.
49. Y. Yuan, J. Liu, B. Gao and M. Sillanpää, *Chemical Engineering Journal*, 444 (2022) 136464.
50. J. Zhang, L. Qi, X. Zhu, X. Yan, Y. Jia, L. Xu, D. Sun and Y. Tang, *Nano Research*, 10 (2017) 3164.
51. M. Yang, C. Li, Y. Zhang, D. Jia, R. Li, Y. Hou, H. Cao and J. Wang, *Ceramics International*, 45 (2019) 14908.
52. J. Rouhi, H.K. Malayeri, S. Kakooei, R. Karimzadeh, S. Alrokayan, H. Khan and M.R. Mahmood, *International Journal of Electrochemical Science*, 13 (2018) 9742.
53. Q. Yang, X. Wu, X. Huang, S. Liao, K. Liang, X. Yu, K. Li, C. Zhi, H. Zhang and N. Li, *ACS Applied Materials & Interfaces*, 11 (2019) 30801.
54. H. Karimi-Maleh, R. Darabi, M. Shabani-Nooshabadi, M. Baghayeri, F. Karimi, J. Rouhi, M. Alizadeh, O. Karaman, Y. Vasseghian and C. Karaman, *Food and Chemical Toxicology*, 162 (2022) 112907.
55. H. Su, Y.-F. Xu, S.-Y. Shen, J.-Q. Wang, J.-T. Li, L. Huang and S.-G. Sun, *Journal of energy chemistry*, 27 (2018) 1637.
56. X. Wang, Z. Qu, T. Lai, G. Ren and W. Wang, *Journal of Power Sources*, 525 (2022) 231121.
57. Z. Zhang, Z. Li, F. Hao, X. Wang, Q. Li, Y. Qi, R. Fan and L. Yin, *Advanced functional materials*, 24 (2014) 2500.
58. P. Bhattacharya, M. Kota, D.H. Suh, K.C. Roh and H.S. Park, *Advanced Energy Materials*, 7 (2017) 1700331.
59. Z. Huang, P. Luo, H. Zheng and Z. Lyu, *JOURNAL OF ALLOYS AND COMPOUNDS*, 908 (2022) 1.
60. M. Yang, C. Li, Y. Zhang, Y. Wang, B. Li, D. Jia, Y. Hou and R. Li, *Applied Thermal Engineering*, 126 (2017) 525.
61. M. Reddy, T. Yu, C.-H. Sow, Z.X. Shen, C.T. Lim, G. Subba Rao and B. Chowdari, *Advanced Functional Materials*, 17 (2007) 2792.
62. W. Cui, X. Li, X. Li, T. Si, L. Lu, T. Ma and Q. Wang, *Journal of Cleaner Production*, 367 (2022) 133031.
63. L. Nan, C. Yalan, L. Jixiang, O. Dujuan, D. Wenhui, J. Rouhi and M. Mustapha, *RSC Advances*, 10 (2020) 27923.
64. C. Luo, Y. Zhu, Y. Xu, Y. Liu, T. Gao, J. Wang and C. Wang, *Journal of Power Sources*, 250 (2014) 372.
65. Z. Zhang, F. Yang, H. Zhang, T. Zhang, H. Wang, Y. Xu and Q. Ma, *Materials Characterization*, 171 (2021) 110732.
66. N. Yan, F. Wang, H. Zhong, Y. Li, Y. Wang, L. Hu and Q. Chen, *Scientific reports*, 3 (2013) 1.
67. M. Yang, C. Li, Y. Zhang, D. Jia, X. Zhang, Y. Hou, R. Li and J. Wang, *International Journal of*

Machine Tools and Manufacture, 122 (2017) 55.
68. S. Changaei, J. Zamir-Anvari, N.-S. Heydari, S.G. Zamharir, M. Arshadi, B. Bahrami, J. Rouhi and R. Karimzadeh, *Journal of Electronic Materials*, 48 (2019) 6216.
69. R. Savari, J. Rouhi, O. Fakhar, S. Kakooei, D. Pourzadeh, O. Jahanbakhsh and S. Shojaei, *Ceramics International*, 47 (2021) 31927.
70. Q. Xiao, Y. Fan, X. Wang, R.A. Susantyoko and Q. Zhang, *Energy & Environmental Science*, 7 (2014) 655.
71. S. Chaudhari and M. Srinivasan, *Journal of Materials Chemistry*, 22 (2012) 23049.
72. L. Zhang, H.B. Wu, S. Madhavi, H.H. Hng and X.W. Lou, *Journal of the American Chemical Society*, 134 (2012) 17388.
73. D. Pan, S. Wang, B. Zhao, M. Wu, H. Zhang, Y. Wang and Z. Jiao, *Chemistry of Materials*, 21 (2009) 3136.
74. B. Wang, J.S. Chen, H.B. Wu, Z. Wang and X.W. Lou, *Journal of the American Chemical Society*, 133 (2011) 17146.
75. H.S. Kim, Y. Piao, S.H. Kang, T. Hyeon and Y.-E. Sung, *Electrochemistry communications*, 12 (2010) 382.
76. F. Han, D. Li, W.C. Li, C. Lei, Q. Sun and A.H. Lu, *Advanced Functional Materials*, 23 (2013) 1692.
77. J. Ji, J. Liu, L. Lai, X. Zhao, Y. Zhen, J. Lin, Y. Zhu, H. Ji, L.L. Zhang and R.S. Ruoff, *Acs Nano*, 9 (2015) 8609.